11th World Congress on Computational Mechanics (WCCM XI)
5th European Conference on Computational Mechanics (ECCM V)
6th European Conference on Computational Fluid Dynamics (ECFD VI)
E. Oñate, J. Oliver and A. Huerta (Eds)

NUMERICAL SIMULATION OF HIGH-SPEED IMPULSIVE NOISE OF THE PZL W-3A "SOKÓŁ" (FALCON) HELICOPTER MAIN ROTOR IN FORWARD FLIGHT

PIOTR DOERFFER[*], OSKAR SZULC[*], FERNANDO TEJERO EMBUENA[*], JERZY ŻÓŁTAK[†] AND JACEK MAŁECKI[+]

[*] The Szewalski Institute of Fluid-Flow Machinery
Polish Academy of Sciences
Fiszera 14, 80-231 Gdańsk, Poland
e-mail: Oskar.Szulc@imp.gda.pl, www.imp.gda.pl

[†] Instytut Lotnictwa (Institute of Aviation)
Aleja Krakowska 110/114, 02-256 Warszawa, Poland
email: geor@ilot.edu.pl, www.ilot.edu.pl

[+] PZL-Świdnik
Aleja Lotników Polskich 1, 21-045 Świdnik, Poland
email: Jacek.Malecki@agustawestland.com, www.pzl.swidnik.pl

Key Words: Helicopter Rotor, High-Speed Impulsive Noise, Chimera Overlapping Grids.

Abstract. The paper presents result of the numerical simulation of the flow and acoustic field generated by the PZL W-3A "Sokół" (Falcon) helicopter main rotor in high-speed forward flight based on the URANS approach and chimera overlapping grids technique. A refined CFD model (40+ million of volumes, 600+ blocks chimera grid) was designed to resolve the flow-field together with the low-frequency content of the acoustic pressure spectrum in the near-field of the rotor blades to allow for the high-speed impulsive (HSI) noise prediction. The detailed, 3d data was recorded for one rotor revolution (approx. 3 TB) allowing exceptional insight into physical mechanisms initiating the occurrence and development of the HSI noise phenomenon.

1 INTRODUCTION

The PZL W-3 "Sokół" (Falcon) is a Polish, medium-size, twin-engine, multipurpose helicopter manufactured by PZL-Świdnik (fig. 1), now member of the British-Italian AugustaWestland company. This first helicopter fully designed and serially built in Poland is still in service since 1987. The original main rotor design has served for more than 25 years and is still operating in hundreds of machines sold all over the world. The increasing significance of the fuel consumption and noise emission restrictions forces the design of an improved version of the helicopter with increased performance and reduced fly-over noise. A completely new, 4-bladed main rotor (based on the ILH family of profiles [1] recently

developed at the Instytut Lotnictwa) for the modernized W-3A "Sokół" (Falcon) helicopter is designed, constructed by the Instytut Lotnictwa and PZL-Świdnik, verified experimentally through scale model wind tunnel tests by the Instytut Lotnictwa in Warsaw (Poland) and tested numerically by the Institute of Fluid-Flow Machinery in Gdańsk (Poland).

Figure 1: PZL W-3A "Sokół" (Falcon) helicopter of the Polish Tatra Volunteer Search and Rescue service

The unrestricted part of the work described in the article contains aerodynamic and aero-acoustic results of a numerical simulation of the original, 4-bladed NACA rotor in high-speed forward flight. During the duration of the project detailed simulations of both rotors NACA and ILH were performed and compared for different low- and high-speed forward flight conditions. The numerical results suggest that the new, ILH rotor is more efficient and emits less noise in flight compared to the older NACA design, but so far the data could not be published due to the confidentiality issues. Hence, the aerodynamic results of the high-speed case will be compared with very limited flight-test data, while for the acoustic part only the CFD results are available and both for the original NACA rotor.

2 PHYSICAL AND NUMERICAL MODELLING

2.1 FLOWer code from DLR

The present investigation was carried out with the FLOWer solver from DLR [2]. It is a modern, parallel, block-structured, cell-centred code solving Favre-averaged Navier-Stokes equations with various turbulence models. The ROT version of the code allows usage of the chimera overlapping grids technique and moving meshes. From various turbulence closures implemented in FLOWer, the two-equation, low-Reynolds k-ω turbulence model of LEA (Linear Explicit Algebraic Stress Model) was chosen [3]. The numerical algorithm uses a semi-discrete approach, utilizing a 2^{nd} order finite-volume formulation for the spatial discretization and a 2^{nd} order implicit dual-time-stepping (with explicit 5-stage Runge-Kutta) method for integration in time. To damp numerical oscillations the scalar artificial dissipation model of Jameson is implemented. A time step equal to the time needed for a rotation by 0.25º degrees of azimuth (1440 time steps per period) and a CFL number ≤ 10.0 for internal R-K stages was set for the dual time-stepping scheme. The density residual gained a drop by 3.0 orders of magnitude within couple of iterations at each physical time step, which proved to be sufficient to obtain accurate unsteady flow field around rotor.

2.2 Rotor geometry

The first approximation is to abandon the influence of the fuselage and tail rotor and to isolate the main rotor blades. The elastic deformation due to air-loads is neglected in the overall picture as well. The rotor of the PZL W-3A "Sokół" (Falcon) helicopter consists of 4 blades (based on the NACA 23012M airfoils) having a radius of R = 7.85 m and linearly twisted from 0º at the root up to -12º at the tip location (fig. 2). Apart from the root, trimming tabs and the tip the chord is equal to c = 0.44 m. The rotor rotates in clock-wise direction as seen from above.

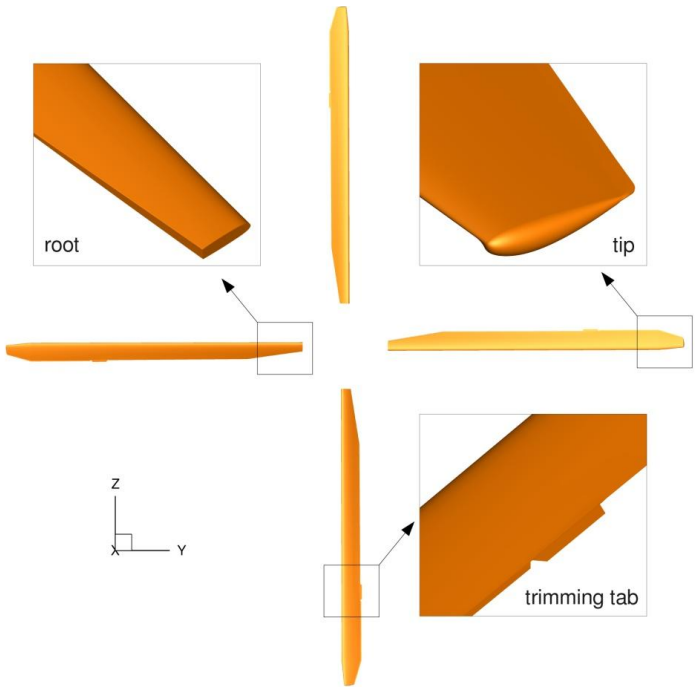

Figure 2: Numerical model of the main rotor of the PZL W-3A "Sokół" (Falcon) helicopter

In forward flight rotor blades not only rotate around the azimuth, but also pitch and flap (lead-lag motion is not considered here). The azimuth angle is assumed to be 0^o for the first blade when it is pointing in the direction opposite to the flight direction. In forward-flight the shaft normal plane is additionally inclined to the flight direction (inflow).

2.3 Chimera component grids

The main idea of the chimera technique [4] implemented in the FLOWer code from DLR is to generate easily grids for complex configurations by decomposing them into simple, independent parts. The only limitation is that all component meshes should overlap each other to allow inter-grid communication. In case of rotors in forward flight the chimera overlapping grids technique allows for an easy control of the rigid motion of the blades (translation, rotation, pitch and flap) preventing any grid deformation. The component overlapped grids for the PZL W-3A "Sokół" (Falcon) helicopter rotor have been generated using the script based approach and Interactive Grid Generator (IGG) from Numeca International allowing for semi-automatic meshing. Three component grids created for a single rotor blade (root, centre and

tip area) are placed within the background, Cartesian mesh. The remaining three blades are generated automatically within the FLOWer solver.

The Cartesian background grid (fig. 3) is designed as a cuboid with dimensions of 16.4 R × 18.2 R × 18.2 R, consequently the far-field surface is located at least 8.0 R away from the rotor in every direction. 32 computational blocks contain $10.35 \cdot 10^6$ volumes (25% of the total number of cells). The core of the background grid surrounding the rotor blades is divided into 4 computational blocks (240 × 240 × 48, $2.8 \cdot 10^6$ volumes) extending beyond the blade tip to 1.1 R and reaching ±0.22 R above and below the rotor plane (fig. 4). The uniform Cartesian grid (dimensions of volumes: 0.16 c × 0.16 c × 0.16 c) located in this refined area constitutes an "acoustic box" designed to support propagation of the acoustic pressure waves resolved in space up to 950 Hz (5 points per wavelength) and detected up to 2380 Hz (2 points per wavelength). Away from the rotor the grid spacing is more relaxed and stretched. The background grid component undergoes only translation with forward flight velocity and a constant tilt by a shaft angle.

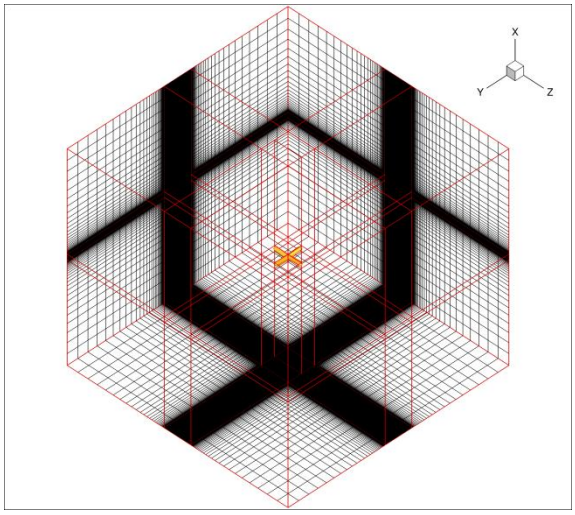

Figure 3: Background component grid

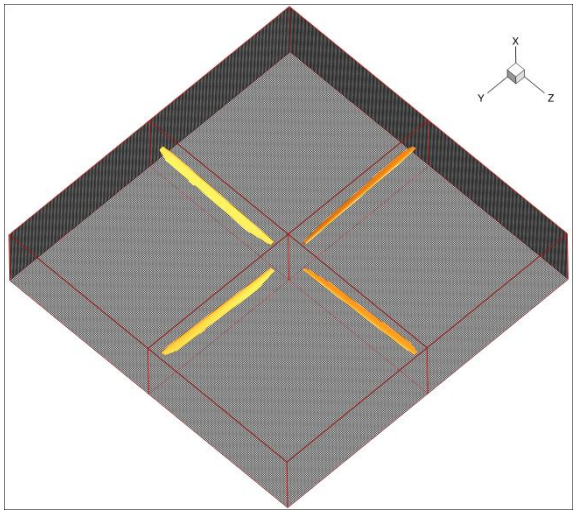

Figure 4: Background component grid – acoustic box

The region of the blade root (fig. 5) is meshed using O-type grid in stream-wise and H-type grid in crosswise directions. It spans from the surface for 2 chord lengths (0.88 m) in the normal direction and 1.5 chords (0.66 m) in the radial direction. It consist of 13 blocks and $1.19 \cdot 10^6$ volumes per blade. The majority of the blade is covered by the blade centre (fig. 6) chimera grid component of a C-type in streamwise and H-type in crosswise directions. It spans from the surface for 2 chord lengths (0.88 m) in the normal direction and consist of 118 blocks and $5.30 \cdot 10^6$ volumes per blade. The close-up at the bottom left corner of fig. 6 reveals the geometrical complexity of the surface mesh and block topology near the trimming tab at the trailing edge of the blade (area depicted in fig. 2 as "trimming tab"). The last component grid covers the area of the blade tip (fig. 7). Due to a rounded tip shape the O-type grid is applied in streamwise and crosswise directions. It spans from the surface for 2 chord lengths (0.88 m) in the normal direction and consist of 19 blocks and $1.08 \cdot 10^6$ volumes per blade. The close-up at the bottom right corner of fig. 7 presents a rounded tip surface mesh in more details (area depicted in fig. 2 as "tip").

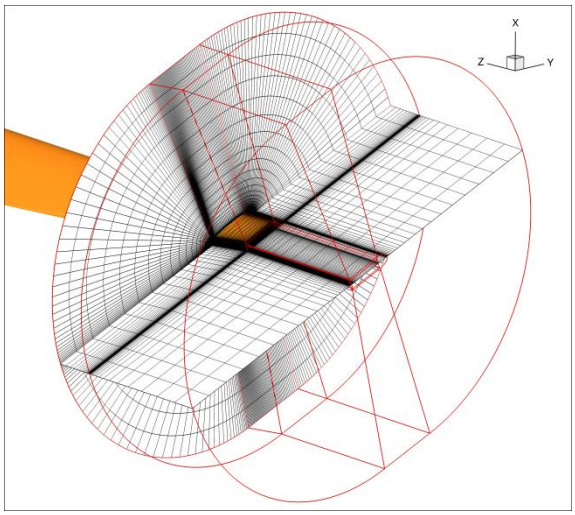

Figure 5: Blade root component grid

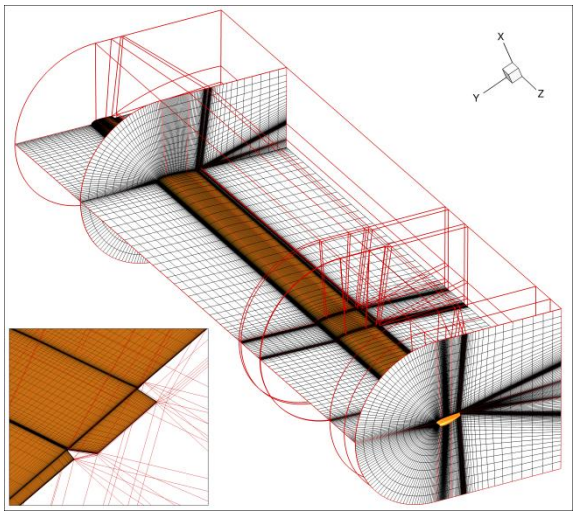

Figure 6: Blade centre component grid

The root, centre and tip components undergo all prescribed motions: translation with forward flight velocity, rotation around the azimuth, a constant tilt by a shaft angle, unsteady pitch and flap. The non-dimensional distance of the first point from the solid surfaces y^+ is of the order of 1.0 for all grids. The complete set of meshes consists of 632 blocks and 40.6 millions of control volumes. The blade component grids (root – green color, centre – red color and tip – blue color) for the first blade are placed in the background grid (fig. 8). The remaining three blades are set-up and managed by the flow solver FLOWer automatically.

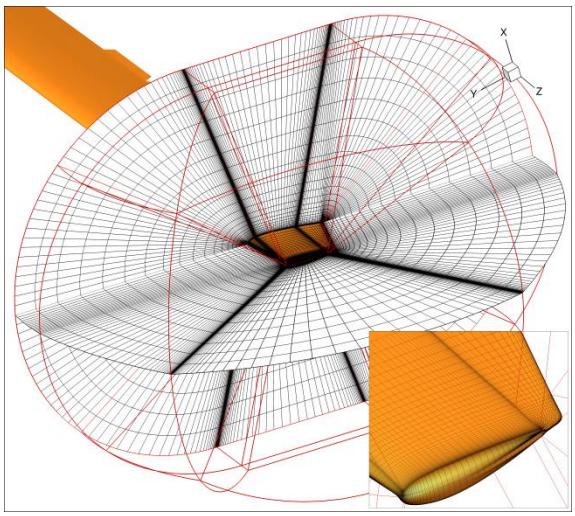

Figure 7: Blade tip component grid

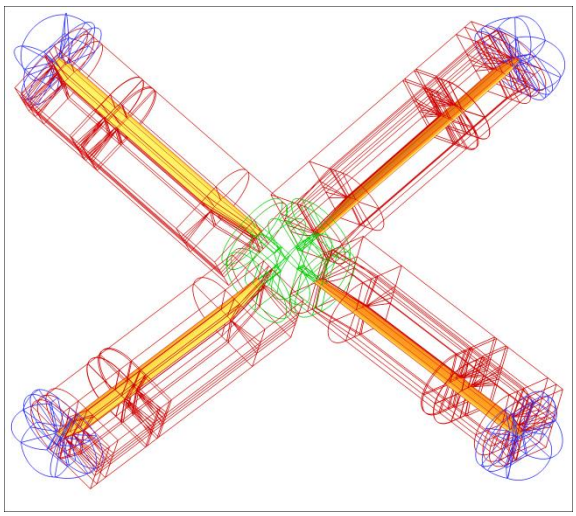

Figure 8: Chimera overlapping grid topology

2.4 Flight test conditions

The high-speed flight test (266 km/h) was realized at 931.0 m above the sea level in the temperature of 5.2 C. The rotor operated at 28.00 rad/s with the tip Mach number of 0.66, tip Reynolds number of $6.3 \cdot 10^6$, forward flight Mach number of 0.22 and forward flight

Reynolds number of $2.1 \cdot 10^6$ (advance ratio of 0.34). During the flight test the instantaneous value of all rotor control angles has been recorded (pitching, flapping and shaft tilt γ according to the flight direction) and are applied in the simulations (more details in [5]).

3 VALIDATION OF THE METHOD

3.1 Caradonna-Tung model helicopter rotor in high-speed hover

The aerodynamic validation of the FLOWer solver applied to rotorcraft flows has been performed against a famous test case of the Caradonna-Tung (C-T) two-bladed model helicopter rotor in high-speed transonic hover operating with a tip Mach number of 0.877 and collective of 8º [6]. The Q-criterion (colored by the vorticity magnitude) visualization of the rotor flow-field and wake (presented in fig. 9) was extracted from the FLOWer numerical solution based on a structured grid and Spalart-Allmaras (SA) turbulence model. On the other hand, the example pressure coefficient distribution C_p obtained using the FLOWer code and the chimera overlapping grids technique (SA turbulence closure) [7, 8] is compared in fig. 10 with the experimental data measured at the chordwise cross-section of the blade r/R = 0.89.

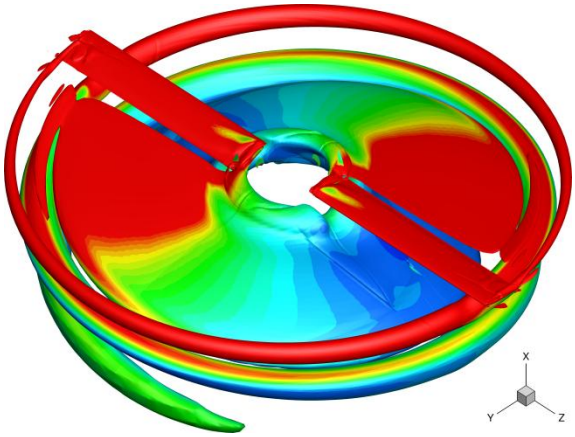

Figure 9: Caradonna-Tung rotor wake

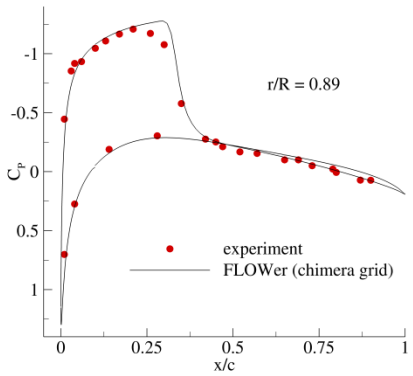

Figure 10: Pressure coefficient distribution

The presented in fig. 9 and fig. 10 solutions based on the structured and chimera grids are of equal quality (compared with the experimental data) as the previous numerical results obtained using other block-structured CFD codes: SPARC [8, 9, 10, 11, 12] and Fine/Turbo from Numeca Int. [8]. The FLOWer results obtained for a hovering C-T rotor using the chimera set-up and LEA k-ω turbulence model (a combination applied for the PZL W-3A "Sokół" (Falcon) helicopter rotor simulations) are validated as well, but presented in [13].

3.2 AH-1G helicopter rotor in high-speed forward flight

The main aerodynamic validation of the forward flight capabilities of the FLOWer code and chimera overlapping grids technique using LEA k-ω turbulence model was performed against the flight test data of the AH-1G helicopter equipped with a 2-bladed, OLS main rotor in low-, medium- and high-speed flight [14]. In high-speed forward flight (295 km/h) the rotor operated with the tip Mach number of 0.64, forward flight Mach number of 0.24

(advance ratio of 0.38). During the flight test the instantaneous values of the total thrust coefficient and pressure coefficient distributions in a few cross-sections of the blade were measured. The recorded rotor control angles (pitch, flap and shaft angle) were applied in the simulation as well. The Q-criterion (colored by the vorticity magnitude) visualization of the flow-field of the rotor at the azymuthal position of 80º was extracted from the FLOWer numerical solution (fig. 11). The example normal force coefficient C_N vs. azymuth and chordwise pressure coefficient C_p distributions are compared with the experimental data measured at r/R = 0.86 (more details in [15]).

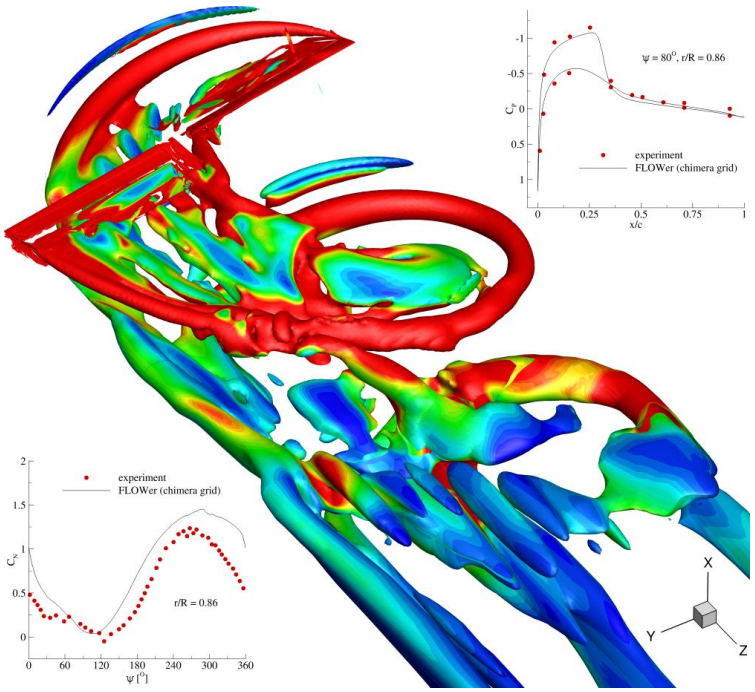

Figure 11: AH-1G helicopter rotor wake, pressure and normal force coefficient distributions

The calculated averaged thrust coefficient is overpredicted by 20%. This leads to the conclusion of a significant influence of the modelling simplifications related to the rigid blade assumption (no flexibility), lack of the fuselage and tail rotor or absence of the main rotor trimming. Still, the data may be used for a comparative study of rotors in terms of the aerodynamic and aero-acoustic performance. In contrary to the low-speed data, the presented CFD results for the high-speed flight test are unique in terms of the literature survey.

4 NUMERICAL RESULTS

4.1 Flow-field of the PZL W-3A "Sokół" (Falcon) helicopter main rotor in high-speed forward flight

The flow-field around the rotor in high-speed forward flight is visualised by an iso-surface of the Q-criterion (colored by the vorticity magnitude) in fig. 12. The blade tip and trimming tabs create strong vortices that interact with the blades leading to the perpendicular and parallel blade-vortex interactions. Due to high relative inflow velocity on the advancing side

large areas of supersonic flow emerge terminated by shock waves, with increasing strength towards the tip. Low angle of attack limits the flow from strong boundary layer separation at this location but shock waves still exist, having a significant impact on the flow and generated high-speed impulsive noise.

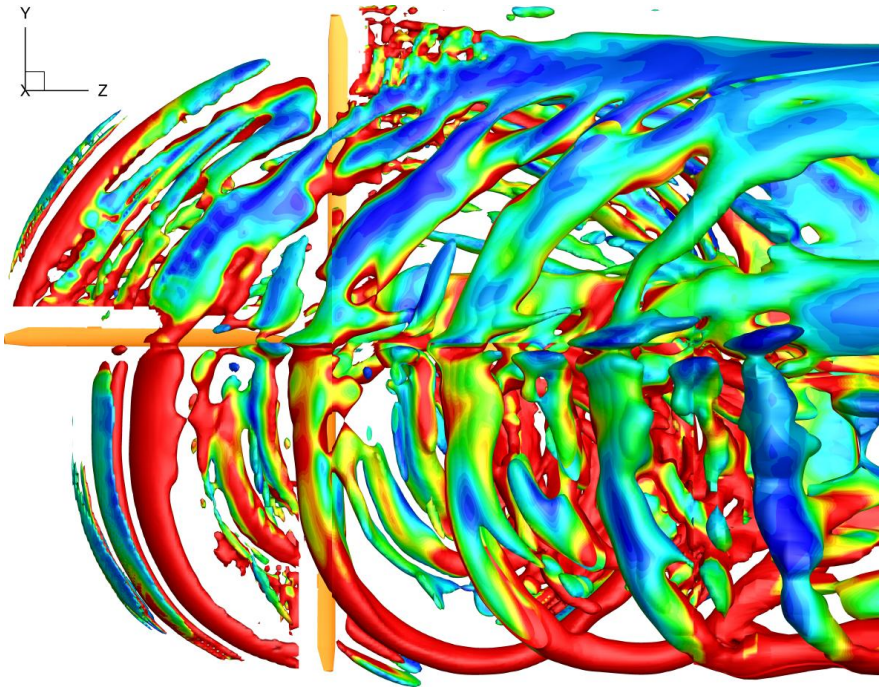

Figure 12: PZL W-3A "Sokół" (Falcon) helicopter rotor wake (as seen from below)

The rotor thrust C_T and power C_P coefficients fluctuate in time with mean values equal to: $C_T = 0.00666$ and $C_P = 0.000705$. The mean component of the force acting against the weight of the helicopter is equal to 7130 kg and the mean power is equal to 2200 HP. It is worth to mention that the PZL W-3A "Sokół" (Falcon) helicopter had a take-off weight of 6100 kg (minus 150 kg of the consumed fuel) and was equipped with engines of the total power equal to 1800 HP. The numerical simulation of the flow past the isolated rotor of the PZL W-3A "Sokół" (Falcon) helicopter in high-speed forward flight leads to the overprediction of the mean thrust and power by ~20% compared to flight test data of the complete helicopter (more details in [5]). It is worth to mention that very similar deviations in the aerodynamic performance were presented in paragraph 3.2 for the numerical simulation of the high-speed forward flight of the AH-1G helicopter main rotor.

4.2 Acoustic field of the PZL W-3A "Sokół" (Falcon) helicopter main rotor in high-speed forward flight

The acoustic post-processing of the CFD simulation was based on the analysis of a big set of the output 3d flow-field data files (3 TB) containing density, pressure and velocity components as well as turbulent quantities. The data was recorded for one rotation period of the rotor every 1º of azimuth (CFD simulation was progressed in time with 0.25º time-step) while keeping the space resolution unmodified. It is worth to mention that the "acoustic box"

uniform grid refinement of the volume enclosing the rotor blades supported propagation of the acoustic pressure fluctuations up to a frequency of 950 Hz (5 points per wavelength) and detection up to a frequency of 2380 Hz (2 points per wavelength). Outside of the "acoustic box" the resolution of the grid was decreasing leading to a strong suppression of the acoustic waves. Since the helicopter high-speed impulsive (HSI) noise phenomenon is low-frequency dominated and emitted mostly in the rotor plane [16] the model constituted a good approximation of the generation and near-field propagation of the acoustic signals.

An example "snaphot" of the acoustic pressure field of the PZL W-3A "Sokół" (Falcon) helicopter rotor in high-speed flight at the plane perpendicular to the shaft and located 0.35 m above the rotor hub is presented in fig. 13. The pressure fluctuations scale was limited from -100 Pa to 100 Pa in order to distinct weak acoustic waves from the very intense background. Due to coning and flapping motion the root and inner part of the blades were located below, while the outer parts and tips were located above the plane. A particularly strong HSI pressure impulse (~140 dB) was generated by the advancing blade at 90º of azimuth and transmitted in the direction forward of the helicopter (marked as "HSI noise" in fig. 13).

To quantify the aerodynamic noise of the rotor the overall sound pressure level OASPL [dB] measure is presented in fig. 14. The averaging process of the root mean square (rms)

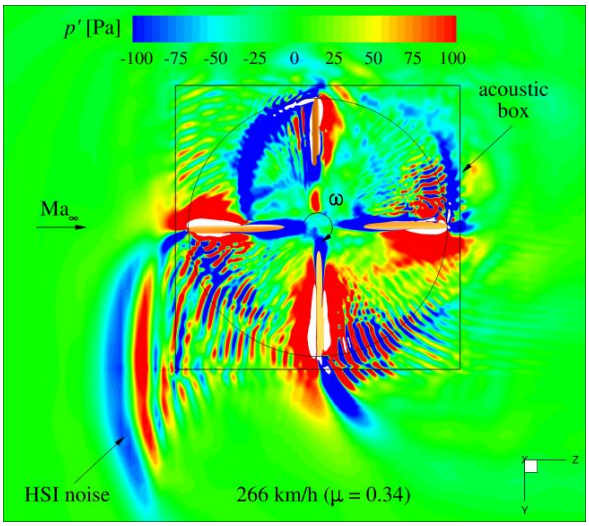

Figure 13: Instantaneous acoustic pressure map

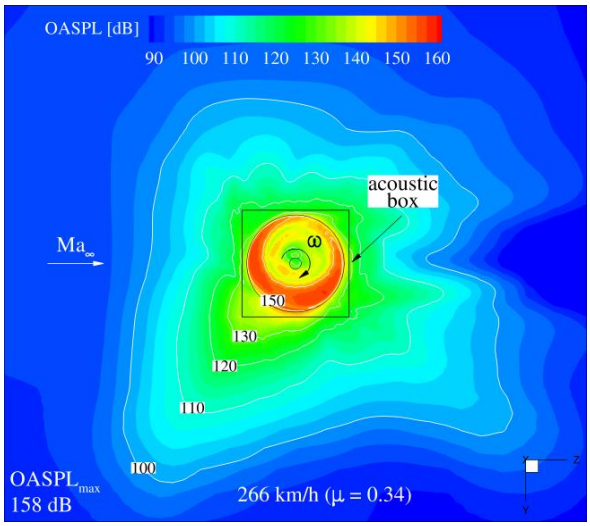

Figure 14: Overall sound pressure level (OASPL)

of the acoustic pressure amplitude was based on the interpolation of the value into a uniform 2d planar grid (2140 × 2140, $4.6 \cdot 10^6$ cells, resolution of 0.1 c) being perpendicular to the shaft and located also 0.35 m above the rotor hub. Due to high advance ratio of 0.34 the OASPL map is highly asymmetrical with higher values shifted to the advancing side of the rotor. The maximum value of the OASPL recorded in the rotor disc at this plane was extremely high and equal to 158 dB, but still lower than the maximum value in the whole volume (161 dB) located at the plane that was crossing the advancing blade tip at 90º of azimuth (0.58 m above the rotor hub). The maximum noise level was decreasing to 145 dB when probing the pressure farther away from the rotor at a circle with a radius of 8.635 m (inscribed in the "acoustic box" at the same plane located 0.58 m above the rotor hub). Already at 5 m from the tip of the

advancing blade at 90º of azimuth the noise level dropped to ~120 dB.

The HSI noise phenomenon is strongly dependent on a relative maximum inflow Mach number present on the advancing blade at 90º of azimuth called Mach attacking Ma_{AT} [17]. The shape and amplitude of the acoustic pulse is changing non-linearly with increasing Ma_{AT}. Below a critical value (called delocalization Mach number) the smooth acoustic waveform is symmetrical (elliptic). Above and at the delocalization Mach number the pulse changes dramatically into a shock waveform (hyperbolic). For the UH-1H helicopter 2-bladed, rectangular and untwisted NACA 0012 rotor operating in non-lifting, hovering conditions the delocalization appears between $Ma_{AT} = 0.88$ and $Ma_{AT} = 0.90$ [18]. For more advanced rotors (in terms of an improved airfoil and blade tip planform, i. e. swept, tapered or thinned) this border is shifted to even higher values of $Ma_{AT} > 0.95$.

In a rotating frame of reference the described change of the noise signature associated with the HSI noise occurs when a local supersonic pocket (relative Mach number $Ma_r > 1.0$) located at the blade tip develops a connection with the non-linear sonic cylinder (surface of a relative Mach number $Ma_r = 1.0$). For this reason, the visualization of the relative Mach number Ma_r is of a great importance in a study of the HSI noise and is presented for the PZL W-3A "Sokół" (Falcon) helicopter rotor in fig. 15. In the analyzed high-speed flight with $Ma_{AT} = 0.88$ the supersonic area ($Ma_r > 1.0$) located near the tip of the advancing blade was not connected with a non-liner sonic cylinder ($Ma_r = 1$) leading to a HSI noise phenomenon far below delocalization.

Apart from the fact that the shock wave was not delocalized, a very intense acoustic pressure pulse was generated by the advancing blade and emitted forward in the direction of the flight of the helicopter. As an example pressure signals recorded at 4 points a_1, r_1, a_2 and r_2 (two on the advancing and two on the retreating side – see fig. 15) in a plane located 0.35 m above the rotor hub are presented in fig. 16. First extraction point a_1 was positioned at the

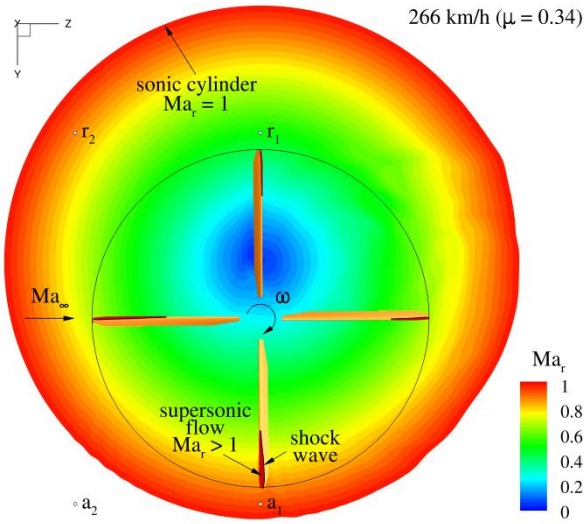

Figure 15: Relative Mach number

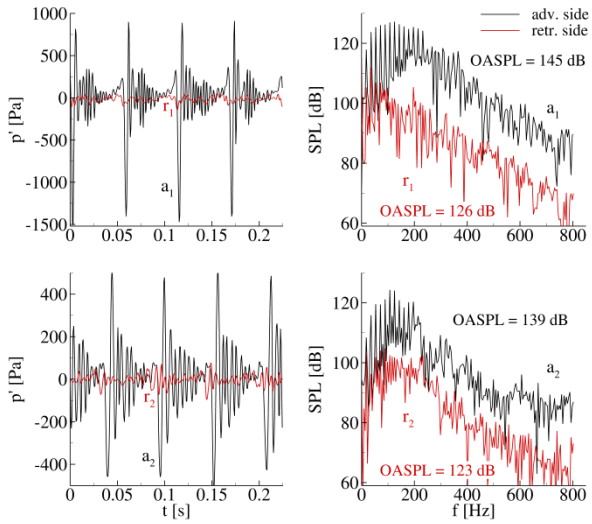

Figure 16: Acoustic pressure and sound pressure level

advancing side at the azimuth of 90º and 8.635 m (r/R = 1.1) from the rotation axis (on the outer edge of the "acoustic box"). The corresponding r_1 point was located on the retreating

side at the azimuth of 270º with the same distance from the rotor axis. The third point a_2 was positioned at the advancing side at the azimuth of 135º and 12.212 m (r/R = 1.556) from the rotation axis (at the bottom left corner of the "acoustic box"). The corresponding r_2 point was located on the retreating side at the azimuth of 225º with the same distance from the rotor axis.

At the blade passing frequency of 17.83 Hz a large pressure peak was visible with an amplitude of more than 1 kPa at point a_1 (source) resulting in the overall sound pressure level (OASPL) of 145 dB. In the same time the amplitude of the pressure peak at point r_1 stayed below 100 Pa with the OASPL of 126 dB. In the area of near-field propagation at point a_2 the amplitude was still large and equal to 500 Pa (OASPL of 139 dB). On the other hand, at the retreating side point r_2 the amplitude was limited to 90 Pa and OASPL of 123 dB. Both spectra recorded at the advancing side points a_1 and a_2 of the sound pressure level (SPL) were dominated by low-frequency content with a maximum energy contained between 20 Hz and 240 Hz. The corresponding points r_1 and r_2 on the retreating side of the rotor were dominated by low frequencies as well. The "spikes" visible in fig. 16 corresponded to the harmonics of the blade passing frequency. The shape of the presented pressure pulses and OASPL spectra are in-line with the experimental observations and flight test data that can be found in the literature (e. g. [16, 18]).

5 CONCLUSIONS

The computational model based on the FLOWer solver, URANS approach and chimera overlapping grids technique was validated and proved to be able to predict complex flow-field of the helicopter rotor in high-speed, transonic hover and forward-flight conditions. Due to a specially prepared background grid the HSI noise phenomenon was predicted together with the flow-field in a single numerical simulation resolving not only the area of the acoustic sources, but the near-field propagation as well. A comparative, aero-acoustic study of a well established rotor of the PZL W-3A "Sokół" (Falcon) helicopter with a completely new design based on the ILH family of airfoil sections was successful, but due to the confidentiality issues has not been presented in the article. The methodology described in the article proved to be very helpful in judging the aero-acoustic noise generated by rotors (NACA and ILH) at the design level of a new version of the PZL W-3A "Sokół" (Falcon) helicopter.

ACKNOWLEDMENTS

The authors would like to thank INTEL Company for providing excellent HPC resources for the numerical simulations described in the paper. We also gratefully acknowledge the help and support provided by Jamie Wilcox from INTEL EMEA Technical Marketing HPC Lab. This research was supported by MNiSW (contract number 03964/C.ZR6-6/2007) and in part by PL-Grid Infrastructure. The research has also received funding from the European Union Seventh Framework Programme (STADYWICO project FP7/2007-2013 under grant agreement no. 251309 and IMESCON project PITN-GA-2010-264672).

REFERENCES

[1] Kania, W. and Stalewski, W. Development of new generation main and tail rotors blade airfoils. *Proceedings of the 22nd Congress of the International Council of the Aeronautical*

Sciences, Harrogate, United Kingdom, 2000.
[2] Rossow, C.-C., Kroll, N. and Schwamborn, D. The MEGAFLOW project – numerical flow simulation for aircraft. In: Di Bucchianico, A., Mattheij, R. M. M., Peletier, M. A. (eds.), *Progress in Industrial Mathematics at ECMI 2004*, vol. 8, pp. 3-33, Springer, 2006.
[3] Rung, T., Lübcke, H., Franke, M., Xue, L., Thiele, F. and Fu, S. Assessment of explicit algebraic stress models in transonic flows. *Proceedings of the 4th International Symposium on Engineering Turbulence Modelling and Measurements*, Ajaccio, France, 1999.
[4] Schwarz, T. The overlapping grid technique for the time accurate simulation of rotorcraft flows. *Proceedings of the 31st European Rotorcraft Forum*, Florence, Italy, 2005.
[5] Szulc, O., Doerffer, P., Żółtak, J. and Małecki, J. Time-accurate simulation of flow past PZL W-3A "Sokół" (Falcon) helicopter main rotor in forward flight, *TASK Quarterly*, vol. 17, no. 1, pp. 43–61, 2013.
[6] Caradonna, F. X. and Tung, C. Experimental and analytical studies of a model helicopter rotor in hover. *NASA Technical Memorandum 81232,* 1981.
[7] Doerffer, P., Tejero E., F. L. and Szulc, O. Numerical simulation of model helicopter rotor in hover using chimera overlapping grids technique, *IMP PAN Report No. 29/2014*, Institute of Fluid-Flow Machinery, Poland, 2014.
[8] Doerffer, P., Szulc, O., Tejero E., F. L. and Martinez S., J. Aerodynamic and aero-acoustic analysis of helicopter rotor blades in hover. In: Bubak, M. (ed.), *E-science on Distributed Computing Infrastructure: PLGrid Plus*, LNCS, Springer, 2014.
[9] Doerffer, P. and Szulc, O. Numerical simulation of model helicopter rotor in hover. *TASK Quarterly*, vol. 12, no. 3, 2008.
[10] Doerffer, P. and Szulc, O. Passive control of shock wave applied to helicopter rotor high-speed impulsive noise reduction. *TASK Quarterly*, vol. 14, no. 3, 2010.
[11] Doerffer, P. and Szulc, O. Application of the passive control of shock wave to the reduction of high-speed impulsive noise. *Journal of Engineering Systems Modelling and Simulation*, vol. 3, no. 1-2, 2011.
[12] Szulc, O. Passive control of shock wave – boundary layer interaction, *Ph.D. Thesis*, Instuitute of Fluid-Flow Machinery, Poland, 2014.
[13] Tejero E., F. L., Doerffer, P., Flaszyński, P. and Szulc, O. Numerical investigation of rod vortex generators on hovering helicopter rotor blade. *Proceedings of the 6th European Conference on Computational Fluid Mechanics*, Barcelona, Spain, 2014.
[14] Cross, J. L. and Watts, M. E. Tip aerodynamics and acoustics test, *NASA Reference Publication 1179*, 1988.
[15] Doerffer, P., Tejero E., F. L. and Szulc, O. Numerical simulation of AH-1G helicopter rotor in forward flight using chimera overlapping grids technique, *IMP PAN Report No. 105/2014*, Institute of Fluid-Flow Machinery, Poland, 2014.
[16] Schmitz, F. H. and Yu, Y. H. Helicopter impulsive noise: theoretical and experimental status. *NASA Technical Memorandum 84390*, 1983.
[17] Yu, Y. H., Park, S. H., Lee, J. W. and Byun, Y. H. Delocalization Mach number in aeroacoustics. Journal of the Korean Physical Society, vol. 51, July, 2007.
[18] Purcell, T. W. CFD and transonic helicopter sound. *Proceedings of the 14th European Rotorcraft Forum*, Milan, 1988.